

1 Long-term NO_x measurements in the remote
2 marine tropical troposphere
3

4 Simone T. Andersen^{1*}, Lucy J. Carpenter¹, Beth S. Nelson¹, Luis Neves², Katie A. Read^{1,3},
5 Chris Reed⁴, Martyn Ward¹, Matthew J. Rowlinson^{1,3}, James D. Lee^{1,3}

6 ¹Wolfson Atmospheric Chemistry Laboratories (WACL), Department of Chemistry,
7 University of York, Heslington, York, YO10 5DD, UK.

8 ²Instituto Nacional de Meteorologia e Geofísica, São Vicente (INMG), Mindelo, Cabo Verde.

9 ³National Centre for Atmospheric Science (NCAS), University of York, Heslington, York,
10 YO10 5DD, UK.

11 ⁴FAAM Airborne Laboratory, Building 146, Cranfield University, Cranfield, MK43 0AL, UK.

12 *Corresponding author: sta516@york.ac.uk
13
14

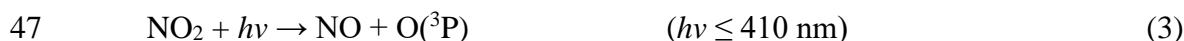
15 Abstract

16 Atmospheric nitrogen oxides ($\text{NO} + \text{NO}_2 = \text{NO}_x$) have been measured at the Cape Verde
17 Atmospheric Observatory (CVAO) in the tropical Atlantic ($16^\circ 51' \text{ N}$, $24^\circ 52' \text{ W}$) since
18 October 2006. These measurements represent a unique time series of NO_x in the background
19 remote troposphere. Nitrogen dioxide (NO_2) is measured via photolytic conversion to nitric
20 oxide (NO) by ultra violet light emitting diode arrays followed by chemiluminescence
21 detection. Since the measurements began, a “blue light converter” (BLC) has been used for
22 NO_2 photolysis, with a maximum spectral output of 395 nm from 2006-2015 and of 385 nm
23 from 2015. The original BLC used was constructed with a Teflon-like material and appeared
24 to cause an overestimation of NO_2 when illuminated. To avoid such interferences, a new
25 additional photolytic converter (PLC) with a quartz photolysis cell (maximum spectral output
26 also 385 nm) was implemented in March 2017. Once corrections are made for the NO_2 artefact
27 from the original BLC, the two NO_2 converters are shown to give comparable NO_2 mixing
28 ratios ($\text{BLC} = 0.99 \times \text{PLC} + 0.7 \text{ ppt}$, linear least squares regression), giving confidence in the
29 quantitative measurement of NO_x at very low levels. Data analysis methods for the NO_x
30 measurements made at CVAO have been developed and applied to the entire time series to
31 produce an internally consistent and high quality long-term data set. NO has a clear diurnal
32 pattern with a maximum mixing ratio of 2-10 ppt during the day depending on the season and
33 ~ 0 ppt during the night. NO_2 shows a fairly flat diurnal signal, although a small increase in
34 daytime NO_x is evident in some months. Monthly average mixing ratios of NO_2 vary between
35 5 and 30 ppt depending on the season. Clear seasonal trends in NO and NO_2 levels can be
36 observed with a maximum in autumn/winter and a minimum in spring/summer.

37

38 1 Introduction

39 Atmospheric nitrogen oxides play a key role in tropospheric chemistry. NO_x helps to
40 control the abundance of the two most important oxidants in the atmosphere, ozone (O_3) and
41 the hydroxyl radical (OH). The presence of NO is usually the key limiting factor in the
42 production of tropospheric O_3 , which occurs via oxidation of NO to NO_2 by peroxy radicals
43 (RO_2 , HO_2) as described in reactions (1-2), followed by photolysis of NO_2 and rapid conversion
44 of the resulting $\text{O}(^3\text{P})$ to O_3 :



49 Reaction (2) also offers a route to the OH radical, above its primary production via O_3
50 photolysis (reactions (5) and (6)). If the NO_x mixing ratio is sufficiently low, then peroxy
51 radicals react with themselves instead of NO, and O_3 depleting reactions (reactions (5) to (8))
52 dominate over O_3 production (Atkinson, 2000).



57 It is assumed that, under tropospheric conditions at the low mole fractions discussed, NO and
58 NO_2 behave as ideal gases and therefore mole fraction (picomole/mole, the appropriate SI unit)
59 is equivalent to volumetric mixing ratio, represented by part per trillion (ppt). NO_x mixing
60 ratios below 10-30 ppt are generally sufficiently low for net tropospheric O_3 depletion
61 (Atkinson, 2000; Jaeglé et al., 1998; Logan, 1985). These conditions have previously been
62 reported to apply most of the year in the remote Atlantic Ocean (Lee et al., 2009). The mixing
63 ratio of NO_x in the atmosphere varies from a few ppt in remote areas (Lee et al., 2009; Monks
64 et al., 1998; Reed et al., 2017) to >100 ppb in polluted areas (Berkes et al., 2018; Carslaw,
65 2005; Mazzeo et al., 2005; Pandey et al., 2008). It is therefore important to have representative

66 NO_x measurements in different regions of the world to be able to understand the chemistry
67 occurring throughout the troposphere.

68 Long-term remote atmospheric NO_x measurements are rare due to the difficulty measuring
69 very low (ppt) mixing ratios. Many different methods of measuring NO_x are available,
70 however, very few have the limit of detection (LOD) and sensitivity needed to measure NO_x
71 in remote regions. The most widely used method is NO chemiluminescence, where NO in the
72 presence of excess ozone is oxidized into excited state NO₂, which emits photons that can be
73 detected (Fontijn et al., 1970). NO₂ is generally converted into NO either catalytically by a
74 heated molybdenum converter or photolytically, followed by NO chemiluminescence (Kley
75 and McFarland, 1980). The molybdenum converter has historically been preferred due to its
76 high conversion efficiency of at least 95%, but it also converts other reactive nitrogen species
77 (NO_z) such as peroxyacetyl nitrate (PAN), peroxyethacryloyl nitrate (MPAN) and other acyl
78 peroxy nitrates (APN), HNO₃, p-HNO₃, HO₂NO₂, and HONO, potentially giving an
79 overestimation of NO₂ (Dunlea et al., 2007; Grosjean and Harrison, 1985; Winer et al., 1974).
80 Two separate studies have shown that photolytic converters (PLC) with a wavelength of 385-
81 395 nm have the smallest spectral overlap with interfering compounds (Pollack et al., 2010;
82 Reed et al., 2016). Reed et al., (2016) showed that in some configurations the PLC can heat up
83 the sampled air making it possible for reactive nitrogen compounds such as PAN to decompose
84 thermally and cause an overestimation of NO₂. This, however, causes only a negligible
85 interference in warm regions such as Cabo Verde where PAN levels are extremely low (Reed
86 et al., 2016).

87 In this study we describe a NO₂ converter, similar to that presented by Pollack et al. (2010),
88 which has been implemented on an instrument to measure NO_x at the CVAO. The data analysis
89 procedure is explained in detail and the first two years of results with the new converter are
90 presented and compared to the data obtained using a different converter.

91

92 2 Experimental

93 2.1 Location

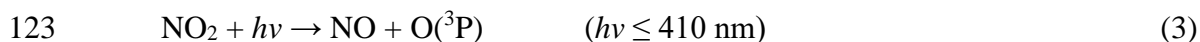
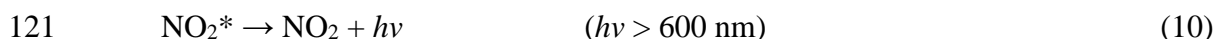
94 The Cape Verde Atmospheric Observatory (CVAO; 16° 51' N, 24° 52' W) is located on
95 the north eastern coast of São Vicente, Cabo Verde. The air masses arriving at the CVAO
96 predominately come from the northeast (>95% of all wind direction measurements, see Figure

97 1) and have travelled over the Atlantic Ocean for multiple days since their last exposure to
98 anthropogenic emissions, with the potential exception of ship emissions (Carpenter et al., 2010;
99 Read et al., 2008). The UK Meteorological Office NAME dispersion model (Ryall et al., 2001)
100 has previously been used to investigate the origin of the air masses arriving at the CVAO,
101 which have been shown to be very diverse; North America, the Atlantic, Europe, Arctic, and
102 African regions (Lee et al., 2009). During the spring and summer, the air masses predominantly
103 originate from the Atlantic making it possible to investigate long-term remote marine
104 tropospheric background measurements. During the winter, the CVAO receives air mainly
105 from the Sahara, resulting in very high wintertime dust loadings (Chiapello et al., 1995; Fomba
106 et al., 2014; Rijkenberg et al., 2008). The time zone of Cabo Verde is UTC-1. A full description
107 of the CVAO site and associated measurements is given in Carpenter et al. (2010).

108

109 2.2 Measurement Technique

110 NO_x has been measured at the CVAO since 2006 using a NO_x chemiluminescence
111 instrument manufactured by Air Quality Design Inc. (AQD), USA. The chemiluminescence
112 technique involves the oxidation of NO by excess O_3 to excited NO_2 (Reaction 9) (Clough and
113 Thrush, 1967; Clyne et al., 1964; Fontijn et al., 1970). The excited NO_2 molecules can be
114 deactivated by emitting photons (Reaction 10) or by being quenched by other molecules
115 (Reaction 11) such as N_2 , O_2 , and in particular H_2O . The emitted photons are detected by a
116 photomultiplier tube detector (PMT), which gives a signal linearly proportional to the mixing
117 ratio of NO sampled. The measurement of NO_x and NO_2 requires photolytic conversion of NO_2
118 to NO (Reaction 3) followed by NO chemiluminescence detection (Kley and McFarland,
119 1980).



124 Further details of the technique are documented in (Carpenter et al., 2010; Drummond et al.,
125 1985; Fontijn et al., 1970; Lee et al., 2009; Peterson and Honrath, 1999; Reed et al., 2017; Val
126 Martin et al., 2006).

127

128 2.3 Instrument Set-up

129 Ambient air is sampled from a downward facing inlet placed into the prevailing wind with
130 a fitted hood 10 m above the ground. A centrifugal pump at a flow rate of ~750 litres per minute
131 pulls the air into a 40 mm glass manifold resulting in a linear sample flow of 10 m s^{-1} , giving
132 a residence time to the inlet of the NO_x instrument of 2.3 s. To reduce the humidity and aerosol
133 concentration in the sampled air, dead-end traps are placed at the lowest point of the manifold
134 inside and outside the laboratory. A Nafion dryer (PD-50T-12-MKR, Permapure) is used to
135 additionally dry the sampled air, using a constant sheath flow of zero air (PAG 003, Eco Physics
136 AG) that has been filtered through a Sofnofil (Molecular Products) and activated charcoal
137 (Sigma Aldrich) trap (dewpoint -15°C). The air is sampled perpendicular to the manifold
138 through a 47mm PTFE (polytetrafluoroethylene) filter with a pore size of $1.2 \mu\text{m}$.

139 A schematic diagram of the instrument is shown in Figure 2. Sampled air is passed through
140 two different photolytic NO_2 converters, which are placed in series. The first is a commercial
141 unit known as a BLC (Blue Light Converter) supplied by Air Quality Design, as described in
142 (Buhr, 2007). An ultra violet light emitting diode (UV-LED, 3 W, LED Engin, Inc.) array is
143 placed in each end of a reaction chamber made of Teflon-like barium doped material (BLC, λ
144 = 385 nm , volume = 16 cm^3). The entire block surrounding the reaction chamber is irradiated,
145 giving the highest possible conversion efficiency of NO_2 . Each array is cooled by a heat sink
146 to maintain an approximately constant temperature inside of the converter when the diode
147 arrays turn on. The second converter consists of two diodes (Hamamatsu Lightningcure
148 L11921-500, $\lambda = 385 \text{ nm}$) and a photolysis cell made of a quartz tube and two quartz windows
149 glued to each end with a volume of 16 cm^3 (PLC) following the design of Pollack et al. (2010).
150 Aluminium foil is wrapped around the quartz tube to increase the reflectivity to give the highest
151 conversion efficiency of NO_2 . The diodes are placed at each end of the quartz tube, as shown
152 in Figure S2, without touching the windows to avoid increases in the temperature when the
153 diodes turn on. BLCs have been used at the CVAO since the instrument was installed in 2006,
154 with the most recent converter installed in April 2015 (a BLC2 model), where the wavelength
155 was changed to 385 nm from 395 nm . The PLC was installed in March 2017. The air flow
156 through the instrument is controlled at $\sim 1000 \text{ sccm}$ by a mass flow controller (MKS, M100B)
157 giving a residence time of 0.96 s through each of the converters.

158 To measure NO and NO_x (NO + NO₂ converted into NO) the air is introduced to the
159 chemiluminescent detector (CLD), where NO is oxidized by excess O₃ into excited NO₂ in the
160 reaction volume (241 mL, aluminium with gold coating (Ridley and Grahek, 1990)) shown in
161 Figure 2. The reaction volume is kept at low pressure to minimize quenching of excited NO₂
162 and thereby maximize the NO chemiluminescence lifetime. The photons emitted from the
163 excited NO₂ molecules when they relax to ground state are detected by the PMT (Hamamatsu
164 R2257P) to give a signal for NO. NO₂ is converted into NO by the BLC for 1 minute, and then
165 the PLC for 1 minute, each period producing a signal due to NO + NO₂. The signal detected
166 by the PMT (S_M) is caused by NO reacting with O₃ (S_{NO}), dark current from the thermionic
167 emissions from the photocathode of the PMT (S_D), and an interference (S_I) which can be due
168 to O₃-surface reactions that cause light emissions in the reaction cell, other reactions creating
169 chemiluminescence, and from illumination of the chamber walls during NO₂ conversion
170 (Drummond et al., 1985; Reed et al., 2016):

$$171 \quad S_M = S_{NO} + S_D + S_I \quad (I)$$

172 The PMT is cooled to -30°C to reduce the dark current, giving the instrument a higher
173 precision. Other molecules in the atmosphere such as alkenes also react with ozone and emit
174 photons to reach their ground state, but at a different time-scale to that of NO₂ (Alam et al.,
175 2020; Finlayson et al., 1974). This can give an interfering signal causing the NO and NO_x
176 mixing ratios to be overestimated. However, most of these reactions emit photons at 400-600
177 nm and are therefore filtered by a red transmission cut-off filter (Schott RG-610) placed in
178 front of the PMT (Alam et al., 2020). The filter transmits photons with a wavelength higher
179 than 600 nm (Drummond et al., 1985). A background measurement is therefore required to
180 account for the dark current of the PMT, O₃-surface reactions, and for the remaining interfering
181 reactions occurring at a different time-scale to that of NO₂. Background measurements are
182 made by allowing ambient air to interact with O₃ in the zero volume (180 mL, PFA, Savillex,
183 LLC) before reaching the reaction volume (Figure 2). Most excited NO₂ molecules will reach
184 their ground state before the sample reaches the PMT, meaning the signal from NO will not be
185 measured. The efficiency of the reaction between NO and O₃ in the zero volume is calculated
186 from the calibration, as explained in section 2.4.3. Background measurements are performed
187 every 5 minutes to take changing ambient conditions such as humidity into account, which can
188 affect the background signal for example via the quantity of light emitted from interference
189 reactions (S_I).

190 NO, NO₂ and the background signal are all detected on the same channel, and the
191 instrument cycle is 1 min of background, 2 min of NO (when the NO₂ converters are off), 1
192 min of BLC NO_x (the BLC converter is on), and 1 min of PLC NO_x (the PLC is on).

193

194 2.4 Calibration

195 Prior to June 2019, calibrations were performed every 73 hours by standard addition in
196 order to account for temperature and humidity changes in the ambient matrix. In June 2019 the
197 calibration frequency was changed to every 61 hours to ensure that during any given month,
198 calibrations are carried out for approximately equal periods during the night and the day. To
199 calibrate the NO sensitivity, 8 sccm of 5 ppm NO calibration gas in nitrogen is added to the
200 ambient air flow of ~1000 sccm, giving an NO mixing ratio of approximately 40 ppb. The
201 mixing ratio used for calibrations are approximately 10,000 times that of the ambient
202 measurements, however, due to reduced cylinder stability for lower NO mixing ratios it is
203 difficult to calibrate at much lower mixing ratios and the chemiluminescence is expected to be
204 linear across the range of expected mixing ratios (Drummond et al., 1985). The calibration gas
205 is added between the PTFE filter and the NO₂ converter as shown in Figure 2. The conversion
206 efficiency of the BLC and the PLC is calibrated by gas phase titration (GPT), where oxygen is
207 added to the sampled NO calibration gas before entering the titration cell, which contains a UV
208 lamp that converts oxygen to ozone. Between 60-80% of the NO calibration gas is oxidized
209 into NO₂, giving a known mixing ratio of NO₂. A theoretical calibration sequence is shown in
210 Figure 3. The first cycle is to calibrate the sensitivity and the second is to calibrate the NO₂
211 conversion efficiency. Each actual calibration includes three cycles of sensitivity calibration
212 and two cycles of conversion efficiency calibration. The signal from NO₂ observed in the NO
213 sensitivity calibration is due to traces of NO₂ in the calibration gas. Figure S3 shows the
214 observed percentage of NO₂ in the calibration cylinders from January 2014 to August 2019
215 calculated from the measured sensitivity (sec. 2.4.1) and the conversion efficiencies (CE) of
216 the two converters (sec. 2.4.2):

$$217 \quad \text{NO}_2 \text{ in cylinder (ppt)} = \frac{(\text{NO}_{c(1)} - \text{NO}_{(1)})}{\text{Sensitivity} \times \text{CE}} \quad (\text{II})$$

$$218 \quad \text{Percentage NO}_2 = \frac{\text{NO}_2 \text{ in cylinder}}{\text{NO}_2 \text{ in cylinder} + \text{NO cal conc.}} \quad (\text{III})$$

219 The percentage is stable for both converters, however, the PLC shows approximately 3-
220 4% NO₂ in the NO calibration gas compared to 5-10% for the BLC, which is caused by a BLC
221 artefact. The cylinders used were certified to ≤2% NO₂.

222

223 2.4.1 Sensitivity

224 The sensitivity of the instrument is calculated from the increase in counts per second
225 caused by the calibration gas during NO calibration (untitrated, i.e. without O₃) and from the
226 mixing ratio of the calibration gas as shown by equation (IV). The NO counts per second from
227 the previous measurement cycle before the calibration is subtracted to give the increase due to
228 the calibration gas. The previous cycle needs to be stable and low in NO to give an accurate
229 sensitivity, which is the case at the CVAO.

$$230 \quad \text{Sensitivity} = \frac{\text{Counts per second during calibration} - \text{Counts per second in previous cycle}}{\text{Mixing ratio of calibration gas}} \quad (\text{IV})$$

231 The sensitivity of the instrument depends on the pressure of the reaction chamber, the
232 ozone mixing ratio in the reaction chamber, the flow of the sample through the reaction
233 chamber, and the temperature of the reaction chamber. To maintain a stable sensitivity, all four
234 parameters should be kept stable (Galbally, 2020). From January 2014 to August 2019 the
235 sensitivity has varied between 2.7 and 7.4 counts s⁻¹ ppt⁻¹ with changes of less than 5% between
236 subsequent calibrations (see Figure S4), unless the instrument has been turned off for a long
237 period of time due to instrumental problems.

238

239 2.4.2 Conversion Efficiencies

240 The conversion efficiency of the BLC and the PLC is calculated based on the titrated (with
241 added O₃) and the untitrated (without added O₃) NO calibration gas as described in equation
242 (V). The numerator gives how much of the NO is titrated into NO₂ and the denominator
243 represents the NO₂ measured when taking the NO₂ content in the NO calibration gas into
244 account. In equation (V), “NO” is the measurement of only NO i.e. when the converters are
245 off, NO.c is when one of the converters are on therefore the measurement is NO + NO₂ and (1)
246 and (2) represent untitrated and titrated NO, respectively.

$$247 \quad \text{CE} = \frac{[(\text{NO.c}_{(2)} - \text{NO}_{(2)}) - (\text{NO.c}_{(1)} - \text{NO}_{(1)})]}{[\text{NO}_{(1)} - \text{NO}_{(2)}]} = 1 - \frac{\text{NO.c}_{(1)} - \text{NO.c}_{(2)}}{\text{NO}_{(1)} - \text{NO}_{(2)}} \quad (\text{V})$$

248 The conversion efficiency of the BLC has varied from 82% to 91% between its installation in
249 April 2015 and August 2019 ($j \sim 3 \text{ s}^{-1}$). Prior to April 2015, an older generation BLC ($\lambda = 395$
250 nm) with a conversion efficiency of 30-35% was used ($j \sim 0.5 \text{ s}^{-1}$). The conversion efficiency
251 of the PLC has varied between 50% and 55% from its installation in March 2017 to August
252 2019 ($j \sim 1 \text{ s}^{-1}$). See Figure S5 for all the calculated conversion efficiencies.

253

254 2.4.3 Efficiency of the Zero Volume

255 Background measurements are made by reacting NO and interference compounds with O₃
256 in the zero volume (Figure 2). The system is set up so that NO₂ produced from NO will relax
257 to the ground state before it is measured in the downstream reaction chamber, whereas it is
258 assumed that any interfering compounds will emit photons when reaching the reaction chamber
259 and be measured as a background signal (Drummond et al., 1985; Galbally, 2020). If the zero
260 volume is too small or the O₃ mixing ratio is too low, some untitrated NO may lead to NO₂
261 chemiluminescence within the reaction chamber and the background will be overestimated. On
262 the other hand, if the zero volume is too large, some of the interfering compounds may have
263 relaxed to their ground state before the reaction chamber and the background signal will be
264 underestimated. The residence time of zero volume is 10.8s compared to 14.5s for the reaction
265 volume. The efficiency of the zero volume can be calculated from the calibration cycle. The
266 difference in background counts from before a calibration cycle to during the calibration cycle
267 shows how much of the added NO from the calibration cylinder does not react with O₃ in the
268 zero volume. By dividing this difference by the signal due to NO during the NO measurement
269 of the calibration cycle, which is obtained by subtracting the NO measurement from the
270 previous measurement cycle, the inefficiency of the zero volume is obtained. The efficiency is
271 determined for each calibration cycle (eq. VI) and plotted in Figure S6. It is consistently above
272 98%.

$$273 \quad \text{Efficiency}_{\text{ZV}} = 1 - \frac{\text{cal zero-measurement zero}}{\text{NO cal-previous NO cycle}} \quad (\text{VI})$$

274

275 2.4.4 Artefact Measurements

276 As described in section 2.3, NO_x measurements may have artefacts from
277 chemiluminescence caused by interfering gas-phase reactions and/or from compounds

278 produced by illumination of the reaction chamber walls as well as from pressure differences in
279 the instrument (Drummond et al., 1985; Reed et al., 2016). To estimate artefacts, it is necessary
280 to measure the signal from NO_x-free air. The calibration sequence is followed by sampling
281 NO_x-free air generated from a pure air generator (PAG 003, Eco Physics AG) for 30 minutes.
282 According to the manufacturer, the PAG not only scrubs NO, NO₂ and NO_y from the ambient
283 air but also SO₂, VOCs, H₂O and O₃. An overflow of PAG air is introduced between the aerosol
284 filter and the NO₂ converters as shown in Figure 2 and the cycle of background, NO, NO_x BLC,
285 and NO_x PLC is used to estimate artefact NO and NO₂ measured by the instrument. The
286 artefacts are estimated using the sensitivity and conversion efficiencies measured in ambient
287 air, where humidity is expected to be higher. This could cause the artefacts to be either under-
288 or overestimated.

289

290 2.4.4.1 NO Artefact

291 The NO artefact can be caused by two things; alkenes reacting with O₃ and giving
292 chemiluminescence above 600 nm at approximately the same rate as NO₂ or a difference in
293 pressure between the zero volume and the reaction volume. An artefact caused by alkenes will
294 be positive and overestimate the NO mixing ratio, where an artefact due to a pressure difference
295 can be either negative or positive. It can be estimated as the offset from 0 ppt when the mixing
296 ratio sampled is 0 ppt. The NO mixing ratio is expected to be 0 ppt when sampling NO_x-free
297 air or between 22.00 and 04.00 UTC at night. NO generated during the day is rapidly oxidized
298 into NO₂ through reactions with O₃ and RO₂ after sunset. During the night, NO is not generated
299 from photolysis of NO₂, and there are no significant local sources of NO at Cabo Verde when
300 the air masses come from over the ocean (which is >95% of the time). The average NO mixing
301 ratio between 22.00 and 04.00 UTC and the average NO mixing ratio from the PAG zero air
302 tend to be very similar, with the PAG artefact (-3.7 ± 22.9 ppt (2σ), January 2014 – August
303 2019) generally lower than the night time artefact (0.4 ± 11.9 ppt (2σ), January 2014 – August
304 2019). Time series of both NO artefact measurements can be found in Figure S7 in the
305 supplementary information. The night time NO artefact is used as it is measured more
306 frequently, it contains the same ambient matrix with nothing scrubbed and to eliminate the
307 possibility of residual NO influencing background measurements determined from the PAG.
308 Since the PAG scrubs VOCs it will also not give an estimate of the artefacts caused by fast
309 reacting alkenes.

310

311 2.4.4.2 NO₂ Artefact

312 NO₂ converters have previously been shown to have artefacts caused by thermal or
313 photolytic conversion of reactive nitrogen compounds (NO_z) other than NO₂ as well as
314 illumination of the chamber walls (Drummond et al., 1985; Reed et al., 2016; Ryerson et al.,
315 2000). Fast reacting alkenes, which can cause overestimations of the NO mixing ratios, will
316 not cause the NO₂ mixing ratio to be overestimated, since the NO signal is subtracted from the
317 NO₂ signal.

318 The spectral output of an NO₂ converter with a wavelength of 385 nm was compared to
319 absorption cross sections of NO₂ and potential interfering species such as BrONO₂, HONO and
320 NO₃ (Reed et al., 2016). The photolytic converter was shown to have good spectral overlap
321 with the NO₂ cross section with minimal spectral overlap with other NO_z species, except for a
322 small overlap with the absorption cross section of HONO. The interference from BrONO₂,
323 HONO and NO₃ have additionally been evaluated previously for a similar set-up using a Hg
324 lamp (Ryerson et al., 2000). At equal concentrations of NO₂ and NO_z species, BrONO₂ and
325 NO₃ were estimated to maximum have an interference of 5% and 10%, respectively, using a
326 lamp with a wider spectral overlap with the interfering species than what is observed for the
327 LEDs used at the CVAO (Ryerson et al., 2000). At the CVAO, HONO levels have previously
328 been measured to peak at ~3.5 ppt (at noon; (Reed et al., 2017)). For the typical Gaussian output
329 of a UV-LED this interference is calculated to be 2.0, 12.6, and 25.7% for UV-LEDs with
330 principle outputs of 395, 385, and 365 nm respectively, resulting in a maximum interference
331 of <0.5 ppt during peak daylight hours. Photolytic conversion of NO_z species is therefore not
332 expected to be an important contributor to the NO₂ artefact at the CVAO due to the narrow
333 spectral output of the LEDs.

334 Each converter is only on for 1 minute in a 5-minute cycle. For thermal conversion to be
335 a major contributor to the artefact, the converter would have to increase in temperature during
336 that one minute and not the rest of the cycle otherwise an increase in signal should be constant
337 since the air continues to flow through the converters when they are turned off. Thermal
338 decomposition of NO_z species is therefore not expected to have an effect in a climate like the
339 one in Cabo Verde, where the sample temperatures are similar to the ambient temperatures.

340 It has been shown that the walls of a BLC made out of a porous Teflon-like doped block
341 becomes contaminated from the ambient air over time, and when the walls are illuminated
342 reactions take place on the surface causing an artefact (Reed et al., 2016; Ryerson et al., 2000).
343 The BLC is similar to the one used by Reed et al. (2016) and it is therefore expected to have
344 an artefact due to reactions taking place on the surface. The PLC is not expected to be
345 contaminated in the same way as it does not have porous chamber walls. Ryerson et al. (2000)
346 observed an increase in artefact over time when sampling ambient air for a similar PLC,
347 however, this is not observed for the PLC in the very clean environment at the CVAO (0-10
348 ppt between August 2017 and August 2019, see below) and surface reactions are therefore
349 expected to give a negligible artefact for the PLC.

350 The total artefact can be determined by measuring the NO₂ signal when the NO₂ mixing
351 ratio is 0 ppt, however, it is virtually impossible to scrub all NO_x from the ambient air and
352 nothing else. To estimate the NO₂ artefact, PAG zero air is measured using both converters.
353 The PLC measures between 0-10 ppt compared to 10-60 ppt using the BLC. Since, as discussed
354 above, the NO₂ artefact of the PLC is assumed to be negligible, the measurement of PAG zero
355 air by the PLC is assumed to represent the remaining NO₂ in the zero air after scrubbing. If the
356 PLC does have an artefact, then both NO₂ measurements will be overestimated by the amount
357 of this artefact. The signal from the BLC when measuring PAG zero air is expected to be due
358 to the illumination of the chamber walls in addition to the traces of NO₂ left in the zero air. The
359 artefact due to wall reactions in the BLC can therefore be estimated by subtracting the signal
360 measured by the PLC.

361

362 3 Data Analysis

363 Time periods with known problems such as maintenance on the manifold, ozone leaks,
364 and periods when the PMT has not reached <-28°C are not included in the dataset. The mean
365 and standard deviation of the zero (background), NO, NO₂ BLC and PLC are determined for
366 each 5-minute measurement cycle. To avoid averaging over the time it takes the detector to
367 change and stabilize between the different types of measurements, the last 50 seconds of the
368 measurement cycle are used for the background and the NO counts, and the last 30 seconds for
369 the BLC NO_x and the PLC NO_x counts. Each cycle is filtered based on the percentage standard
370 deviations and differences in counts between subsequent cycles. If the standard deviation or
371 the difference in counts are outside the mean $\pm 2\sigma$ (see Table 1) calculated from a 5-year period

372 between 2014 and 2018, the cycle is not used for further analysis. This removes noisy data as
373 well as sharp spikes but keeps data with sustained increases lasting more than 5 minutes.

374 To obtain the signals due to NO and NO₂, the interpolated zero and NO measurements are
375 subtracted from the NO and NO_x measurements, respectively. They are converted to a
376 concentration by using the interpolated sensitivity and conversion efficiency as shown in
377 equation VII and VIII:

$$378 \quad \text{NO mixing ratio} = \frac{\text{NO measurement} - \text{background measurement}}{\text{Sensitivity}} \quad (\text{VII})$$

$$379 \quad \text{NO}_2 \text{ mixing ratio} = \frac{\text{NO}_x \text{ measurement} - \text{NO measurement}}{\text{Sensitivity} \times \text{CE}} \quad (\text{VIII})$$

380 The NO and NO₂ BLC concentrations are corrected by subtracting the interpolated
381 artefacts described in sections 2.4.4.1 and 2.4.4.2. If the difference between two subsequent
382 NO artefact measurements vary by more than the mean $\pm 2\sigma$ of the differences in NO artefacts
383 determined from January 2014 – August 2019 (0.0 ± 6.2 ppt), the measurements made between
384 are not used for further analysis due to a potential step change between the determinations.

385 Hourly averages of all the measurements are determined. If data coverage during the hour
386 is less than 50%, the hour is flagged and discarded from the data analysis. The hourly NO_x (NO
387 + NO₂ PLC) concentrations between June 2017 and August 2019 are plotted as a function of
388 wind speed and direction in figure 4. It can be observed that the concentrations are enhanced
389 at low wind speed and when the air crosses the island (from the southwest). Measurements
390 made at a wind speed <2 m/s or from a wind direction 100-360° are, therefore, flagged as
391 suspected of local contamination and are not used in the analysis. Extreme mixing ratios outside
392 the mean $\pm 4\sigma$ of the 5-year for NO and 2-year period for NO₂ are flagged as suspicious (see
393 Table 1 for boundaries). Lastly, inconsistency in the measurements such as differences outside
394 the mean $\pm 4\sigma$ between the mean and median of a measurement (see Table 1 for boundaries)
395 and differences between the two NO₂ measurements are flagged as suspicious (0.4 ± 32.2 ppt).
396 The data remaining after these removals are 88% of the original NO and NO₂ BLC dataset and
397 83% of the NO₂ PLC dataset remain to analyse.

398

399 3.1 Corrections

400 As described above, excited NO₂ can be quenched by other sampled molecules, giving a
 401 lower observed mixing ratio than the real value. Water molecules are effective quenchers and
 402 therefore a correction is usually applied depending on the humidity (Matthews et al., 1977;
 403 Ridley et al., 1992). However, since the calibrations at the CVAO are performed by standard
 404 addition, and a Nafion dryer is placed in front of the instrument, this is not necessary.

405 Additionally, NO can react with O₃ in the ambient air in the inlet and manifold giving an
 406 overestimation of NO₂ and an underestimation of NO. To correct for this the following
 407 equations are used (Gilge et al., 2014):

$$408 \quad [\text{NO}]_0 = [\text{NO}]_{\text{E1}} \times e^{k_{\text{O}_3} \times t_{\text{E1}}} \quad (\text{IX})$$

$$409 \quad [\text{NO}_2]_0 = \left(\frac{J_{\text{C}} + k_{\text{O}_3}}{J_{\text{C}}} \right) \times \left(\frac{[\text{NO}]_{\text{E2}} - [\text{NO}]_{\text{E1}} \times e^{-(k_{\text{O}_3} \times (t_{\text{C2}} - t_{\text{C1}}) + J_{\text{C}} \times t_{\text{C2}})}}{1 - e^{-(k_{\text{O}_3} + J_{\text{C}}) \times t_{\text{C2}}}} \right) - [\text{NO}]_0 \quad (\text{X})$$

410 where [NO]₀ is the corrected NO mixing ratio, [NO]_{E1} is the uncorrected NO mixing ratio,
 411 [NO₂]₀ is the corrected NO₂ mixing ratio, [NO]_{E2} is the uncorrected NO mixing ratio when the
 412 converter is on, *k*_{O₃} is the rate of the reaction between NO and O₃ (*k*(O₃+NO) × [O₃] × 10⁻⁹ ×
 413 M), *t*_{E1} is the sum of the residence time from the inlet to entry of the converter and the time the
 414 air is in the converter, *t*_{C1} and *t*_{C2} are the time the air is in the converter when the converter is
 415 on and off, respectively, and *J*_C is the photolysis rate inside the converter. The residence time
 416 from the inlet to the entry of the converter has been 2.3 s since 2015 and the time the air is in
 417 each of the converters is 1.0 s (with and without the converter on). The O₃ mixing ratio
 418 measured at the CVAO has varied between 5 and 60 ppb (with an uncertainty of 0.07 ppb)
 419 between 2014 and 2019. The ozone correction is calculated for each hour using a rate
 420 coefficient of 1.8 × 10⁻¹⁴ cm³ molecule⁻¹ s⁻¹ at 298K (Atkinson et al., 2004). This gives an
 421 average O₃ correction ± 2σ of 6.8 ± 3.0%, 1.7 ± 11.0%, and 1.3 ± 7.1% for NO, NO₂ BLC, and
 422 NO₂ PLC, respectively, when the mixing ratio measured is above 0.1 ppt (See supplementary
 423 information for an example of the calculation). Thus, at the low mixing ratios of O₃ present at
 424 Cabo Verde and the short residence time for sampling, the corrections for O₃ are well within
 425 the noise of the measurements (see below), but are still included in the final calculated mixing
 426 ratios.

427

428 4 Uncertainty Analysis

429 To be able to evaluate the NO_x measurements made at the CVAO an extensive uncertainty
430 analysis is performed. A summary of the analysis can be found in Table 2 and a detailed
431 description in the supplementary information. The hourly precision and uncertainty of the
432 instrument are estimated to characterize the uncertainties at the 95 percent confidence interval
433 (Bell, 2001). The hourly precision is estimated from the zero count variability, which is directly
434 related to the photon-counting precision of the PMT. The uncertainty of the hourly
435 measurements is estimated by combining all the uncertainties associated with the
436 measurements. This includes uncertainties in the calibrations, artefact determinations, and O₃
437 corrections as well as the precision of the instrument. The precision of the NO and NO₂
438 measurements are both included in the total uncertainty of the NO₂ measurements as the NO
439 measurements are subtracted from the NO₂ measurements. Each term is converted into ppt to
440 be able to combine them using error propagation.

441 The 2 σ precision for hourly averaged NO data between January 2014 and August 2019 is
442 1.0 ± 0.9 ppt. The hourly precisions reported here are in good agreement with our previously
443 reported 1 σ precision of the instrument of 0.30 ppt (Reed et al., 2017) and the 2 σ precision of
444 0.6-1.7 ppt (Lee et al., 2009). The NO₂ precisions are determined by taking the conversion
445 efficiency of the respective converters into account. The hourly 2 σ precision for hourly
446 averaged NO₂ data between March 2017 and August 2019 becomes 1.5 ± 0.8 ppt and 2.7 ± 2.2
447 ppt for the BLC and PLC, respectively. The determined NO₂ precisions are within the interval
448 of previously reported precisions for the same instrument (Lee et al., 2009; Reed et al., 2017).

449 The total hourly uncertainty for each of the three measurements are determined by
450 combining all the uncertainties described using propagation of uncertainties. The precisions
451 are already calculated as hourly precisions in ppt. The calibration uncertainties are interpolated
452 between each calibration and multiplied by the hourly concentrations of NO and NO₂ to
453 calculate hourly uncertainties in ppt. The artefact uncertainties are interpolated between each
454 artefact determination, and the uncertainty due to ozone corrections is determined by
455 multiplying the % uncertainties by the hourly concentrations of NO and NO₂. The hourly
456 uncertainties are determined to be 1.4 ± 1.5 ppt, 8.4 ± 7.5 ppt, and 4.4 ± 5.8 ppt for NO, NO₂
457 BLC, and NO₂ PLC, respectively.

458

459 5 Results: Examples of Data

460 The first year of data (August 1st 2017 to July 31st 2018) is chosen as an example of the
461 resulting NO and NO₂ datasets. October 2017, December 2017, and April 2018 are used to
462 highlight the seasonality in the mixing ratios observed during a year of measurements. Panel
463 A in figure 5 and 6 show the full O₃ corrected time series for NO and NO₂, respectively. Panel
464 B, C, and D in the two figures show the time series for the three chosen months and panel E,
465 F, and G show the 3-hour rolling average diurnals for the same months. Monthly diurnals for
466 NO and NO₂ for the entire year can be found in figure S9 and S10, respectively.

467 Clear seasonality can be observed in the diurnal cycles of NO measurements with a
468 maximum of ~10 ppt in Winter and a minimum of ~2 ppt in the spring and summer. This is in
469 good agreement with that reported for previous years (Lee et al., 2009; Reed et al., 2017). The
470 two NO₂ measurements are in general in good agreement when looking at the time series in
471 figure 6. Offsets of up to 10 ppt between the two measurements can be seen over some time
472 periods (E.g. April, Panel D), which are most likely caused by the calculated BLC artefact for
473 those periods either being too high or too low. This is supported by the diurnals having the
474 same shape, but with an offset. Monthly diurnals of the two NO₂ measurements agree within 2
475 standard errors except in August 2017, where the offset between the two measurements is larger
476 than for the remaining months. NO₂ shows a fairly flat diurnal signal, although a small increase
477 in daytime NO₂ is evident in some months, which is in agreement with that reported for
478 previous years (Lee et al., 2009; Reed et al., 2017). Spikes in the early morning are noticeable
479 in the NO₂ diurnals for July-November, which correspond to the months with an average lower
480 wind speed than the rest of the year (the diurnal for April also shows a spike, however, it is
481 caused by data from one morning). These spikes could be caused by local fishing boats passing
482 upwind of the observatory in the morning hours, which will give a more prominent spike a low
483 wind speed. Monthly wind speed diurnals can be found in figure S11. The good agreement
484 between the two NO₂ measurements observed in figure 6 can also be observed in figure 7,
485 where the two are plotted against each other. The data points are scattered around the 1:1 line
486 shown in black. A linear least squares regression (with uncertainty in the BLC measurements)
487 and an orthogonal distance regression (ODR) (with uncertainty in both measurements) are
488 performed to evaluate the scatter of the data points between August 2017 and 2019. The
489 resulting regression lines are displayed in red (BLC = $0.99 \times \text{PLC} + 0.7$ ppt) and blue (BLC =
490 $1.08 \times \text{PLC} - 0.6$ ppt). The deviation in the slope from 1 for both regressions are consistent

491 with the uncertainty in the measured NO₂ artefact which has been determined to be 7.2 ± 7.2
492 ppt.

493 The seasonality of the NO measurements can be explained by a combination of the
494 variation of the origin of the air masses arriving at the CVAO, meteorology, photolysis rates,
495 and seasonality of emissions. Back trajectories of the three months used as examples are shown
496 in figure 8. FLEXPART version 10.4 is used in backwards mode, driven by pressure level data
497 from Global Forecast System (GFS) reanalyses at 0.5°×0.5° resolution (Pisso et al., 2019; Stohl
498 et al., 1998). 10-day back-trajectory simulations are initialised every 6 hours, releasing 1000
499 particles from the CVAO site. Further information on FLEXPART can be found in the
500 supplementary information. During the winter maximum (December) the back-trajectories
501 indicate that the air reaching CVAO is largely dominated by African air, compared to during
502 the spring minimum (April), which is dominated by Atlantic marine air. Large west African
503 cities such as Dakar and Nouakchott, and/or the shipping lanes to the east/northeast of Cabo
504 Verde, are potential candidates for the source of elevated NO_x. The NO mixing ratios measured
505 in October are higher than those in April and lower than in December. This may be due in part
506 to the influence of polluted African air arriving at Cabo Verde, which is more prominent in
507 October than in April, but less so than in December. The NO₂ and the total NO_x (NO + PLC
508 NO₂, figure 9) similarly show higher levels in December than April, but the mixing ratios
509 observed in October are similar to those in April. It should be noted that some of the days with
510 high percentages of African air have missing data or wind directions from other places than the
511 north east.

512 From table 3 it can be observed that the NO, NO₂, and NO_x measurements at the CVAO
513 compare well to the few other measurements in the remote marine boundary layer as well as
514 background sites in Alert, Canada and measurements in the free troposphere. A wintertime
515 seasonal increase in NO, NO₂, and NO_x can be observed during December-February, which
516 corresponds to the months when surface air masses arrive at Cabo Verde from western Africa
517 (Carpenter et al., 2010; Lee et al., 2009).

518

519 6 Conclusion

520 NO₂ was measured at a remote marine site by photolytic conversion to NO followed by
521 chemiluminescence detection, using two different methods for conversion. A photolytic NO₂

522 converter with external diodes and a quartz photolysis cell (PLC) has been installed at the Cape
523 Verde Atmospheric Observatory and the NO₂ measurements have been compared to those of
524 the historical BLC used at the site, which has internal diodes and a reaction chamber made of
525 Teflon-like barium doped material. The two measurements show good agreement (BLC = 0.99
526 × PLC + 0.7 ppt, linear least squares analysis) with small differences due to uncertainties in the
527 estimations of the BLC NO₂ artefact. Even though the PLC has a lower conversion efficiency
528 (CE= 52 ± 4%) than the BLC (CE= 85 ± 4%), it is preferred due to its assumed negligible
529 artefact as a consequence of having non-porous/non-reactive walls. The assumption of a zero
530 artefact causes the hourly uncertainty of the NO₂ measurements to be roughly halved. With 2σ
531 hourly precisions of 1.0 ± 0.9 ppt, 1.5 ± 0.8 ppt, and 2.7 ± 2.2 ppt and 2σ hourly uncertainties
532 of 1.4 ± 1.5 ppt, 8.4 ± 7.5 ppt, and 4.4 ± 5.8 ppt for NO, NO₂ BLC, and NO₂ PLC, respectively,
533 the instrument has a high repeatability and low uncertainties for all the measurements. The
534 mixing ratios observed at the CVAO (NO: 2-10 ppt, NO₂: 5-50 ppt, and NO_x: 7-60 ppt at
535 midday) are in good agreement with previous measurements at the CVAO as well as other
536 remote measurements around the world.

537

538 7 Data availability

539 The processed data is available through Ebas

540 (<http://ebas.nilu.no/Pages/DataSetList.aspx?key=45DB99FE2B7F4F97864ECF800E71E5D5>

541) and through CEDA (Center for Environmental Data Analysis,

542 <https://catalogue.ceda.ac.uk/uuid/d5422d54d519ed056cc17e97037732b8>).

543

544 8 Author contribution

545 LN runs the instrument on a day-to-day basis. MW and STA wrote the script processing the
546 data. MJR ran the back-trajectory analysis. BSN developed the photolytic converter setup. All
547 authors were involved in the analysis, data evaluation and discussion of the results. STA wrote
548 the paper with contributions from all coauthors. All coauthors proofread and commented on
549 the paper.

550

551 **9 Competing interests**

552 The authors declare that they have no conflict of interest.

553

554 **10 Acknowledgements**

555 The authors would like to thank Franz Rohrer (Forschungszentrum Jülich) and Tomás Sherwen
556 (University of York) for scientific discussions, and the UK National Environment Research
557 Council/ National Centre for Atmospheric Science (NERC/NCAS) for funding the CVAO
558 programme. STA's PhD was funded through the NERC SPHERES Doctoral Training
559 Partnership and the University of York.

11 Tables

Table 1: Evaluation parameters of the measurements. When a measurement falls outside any of the intervals it will not be used for further data analysis. The mean $\pm x\sigma$ is calculated for 2014-2019 for the zero and NO measurements, and 2017-2019 for both NO₂ measurements.

Measurement	Standard deviation of a measurement cycle (mean $\pm 2\sigma$, %)^a	Difference in counts/s between subsequent cycles (mean $\pm 2\sigma$)	Hourly mean $\pm 4\sigma$ (ppt)^b	Difference between mean and median (mean $\pm 4\sigma$, ppt)^c
Zero	2.4 \pm 1.7	-	-	-
NO	2.5 \pm 10.6	0 \pm 515	1.7 \pm 47.9	0.2 \pm 4.1
NO ₂ BLC	2.5 \pm 7.5	0 \pm 1432	16.8 \pm 175.2	1.5 \pm 33.0
NO ₂ PLC	2.1 \pm 2.5	0 \pm 738	17.3 \pm 176.8	1.7 \pm 33.0

^aThe percentage standard deviation for each measurement cycle is determined as the standard deviation of a cycle divided by the mean of the same cycle. ^bExtreme measurements are determined to be mixing ratios, which are outside the hourly mean ± 4 standard deviations of the hourly mixing ratio. ^cExtreme differences between the hourly mean and median of the mixing ratios are determined to be differences outside the hourly mean ± 4 standard deviations of the differences between the mean and median.

Table 2: Calculated uncertainties associated with the NO_x measurements. The values in bold are the combined uncertainties for each type of measurement. Each uncertainty is given as the mean uncertainty \pm 2 standard deviation of the data between January 2014 and August 2019 for NO and from March 2017 to August 2019 for both NO₂ measurements.

Source of uncertainty	Probability distribution	Uncertainty (%)	Uncertainty (ppt)
Hourly precision/repeatability NO	Normal		1.0 \pm 0.9
Hourly precision/repeatability NO ₂ BLC	Normal		1.5 \pm 0.8
Hourly precision/repeatability NO ₂ PLC	Normal		2.7 \pm 2.2
Total Calibration uncertainty NO ^a		2.78 \pm 8.05	0.0 \pm 0.3
Total Calibration uncertainty NO ₂ BLC ^a		3.44 \pm 9.32	0.3 \pm 1.3
Total Calibration uncertainty NO ₂ PLC ^a		3.52 \pm 8.67	0.4 \pm 1.3
Total NO artefact uncertainty ^b			1.1 \pm 3.4
Total NO ₂ artefact uncertainty ^b			7.2 \pm 7.2
Hourly O ₃ correction uncertainty NO	Normal	20.00 \pm 0.001	0.3 \pm 1.1
Hourly O ₃ correction uncertainty NO ₂ BLC	Normal	20.00 \pm 0.001	2.5 \pm 6.8
Hourly O ₃ correction uncertainty NO ₂ PLC	Normal	20.00 \pm 0.001	2.6 \pm 6.4
Total hourly uncertainty NO			1.4 \pm 1.5
Total hourly uncertainty NO ₂ BLC			8.4 \pm 7.5
Total hourly uncertainty NO ₂ PLC			4.4 \pm 5.8

^aThe individual uncertainties associated with the calibration can be found in table S1. ^bThe individual uncertainties associated with the artefact determination can be found in table S2.

Table 3: NO, NO₂, and NO_x mixing ratios at different low NO_x sites.

	NO (ppt) ^k	NO ₂ (ppt)	NO _x (ppt)	Reference
Tropospheric Marine				
CVAO, Cape Verde 2017-2018	2-10	5-50	7-60	This study
Cape Grim, Australia ^a	1-6	3-6	4-12	(Monks et al., 1998)
SAGA3, Pacific Ocean, Cruise ^b	2.9 ± 0.1			(Torres and Thompson, 1993)
ASTEX, North Atlantic, Cruise ^c	5 ± 4	29 ± 8		(Carsey et al., 1997)
WOCE, Indian Ocean, Cruise ^d	~ 5	18-40		(Rhoads et al., 1997)
Background Sites				
Alert, Canada ^e	0.2-2.8	1.3-10.8		(Beine et al., 2002)
South Pole ^f	~ 10			(Jones et al., 1999)
Free Troposphere				
Mauna Loa, USA ^g	9.4	29.6	32	(Carroll et al., 1992)
Pico Mountain, Portugal ^h	0-9	19-30	20-37	(Val Martin et al., 2008)
NASA GTE, Pacific Ocean, Aircraft ⁱ	~ 1			(Ridley et al., 1987)
Svalbard, Norway ^j			27.7 ± 24.0	(Beine et al., 1996)

^aMeasurements made during the SOAPEX (Southern Ocean Atmospheric Photochemistry EXperiment) campaign during Austral summer in 1995. ^bMeasurements from the Soviet-American Gases and Aerosols (SAGA) campaign between Hawaii and American Samoa between February and March. ^cMeasurements from 6 clean days on the Atlantic Stratocumulus Transition Experiment (ASTEX). ^dMeasurements from the World Ocean Circulation Experiment (WOCE) between South Africa and Sri Lanka. ^eMeasurements made during 24-hour darkness and in spring. ^fMeasurements made from January-March 1997 at the German Antarctic research station, Neumayer. ^gMeasurements made during the Mauna Loa Observatory Photochemistry Experiment (MLOPEX) in May 1988. ^hMeasurements made at Mount Pico between July 2002 and August 2005. ⁱMeasurements made in the upper marine boundary layer from 13 flights between California and west of Hawaii. ^jMeasurements made at the Ny-Ålesund Zeppelin mountain station on Svalbard during a spring campaign in 1994. ^kDaytime values.

12 Figures

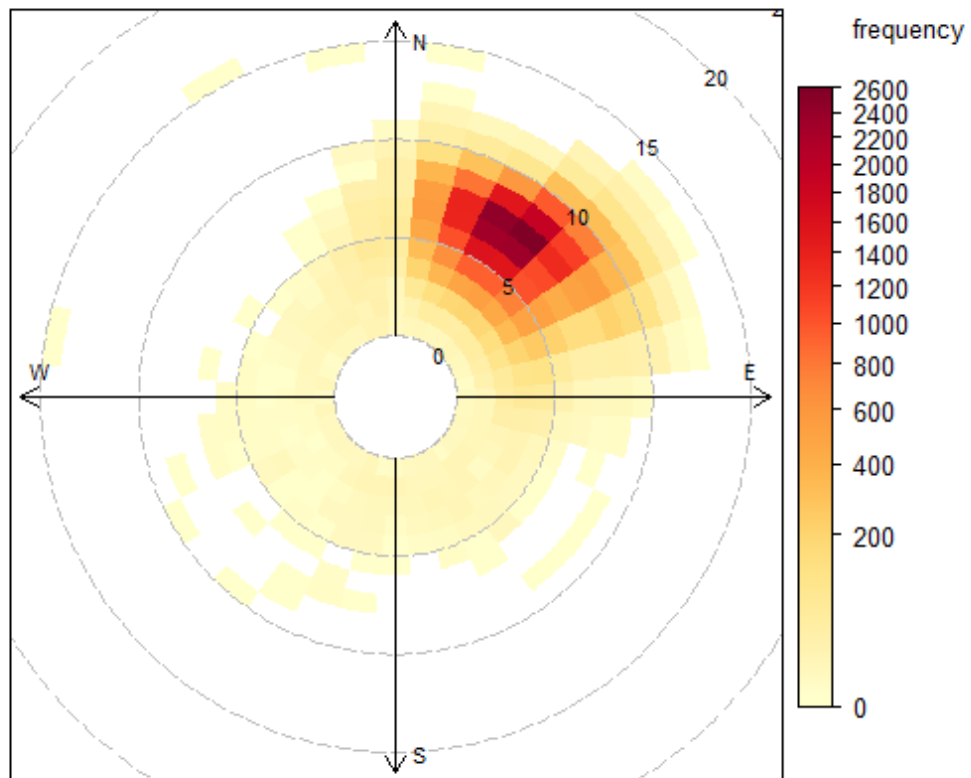


Figure 1: The frequency of hourly averaged wind speed and direction from January 2014 to August 2019. Each square symbolises 10 degrees of wind direction and 1 m/s wind speed. Each dashed circle shows an increase in wind speed of 5 m/s.

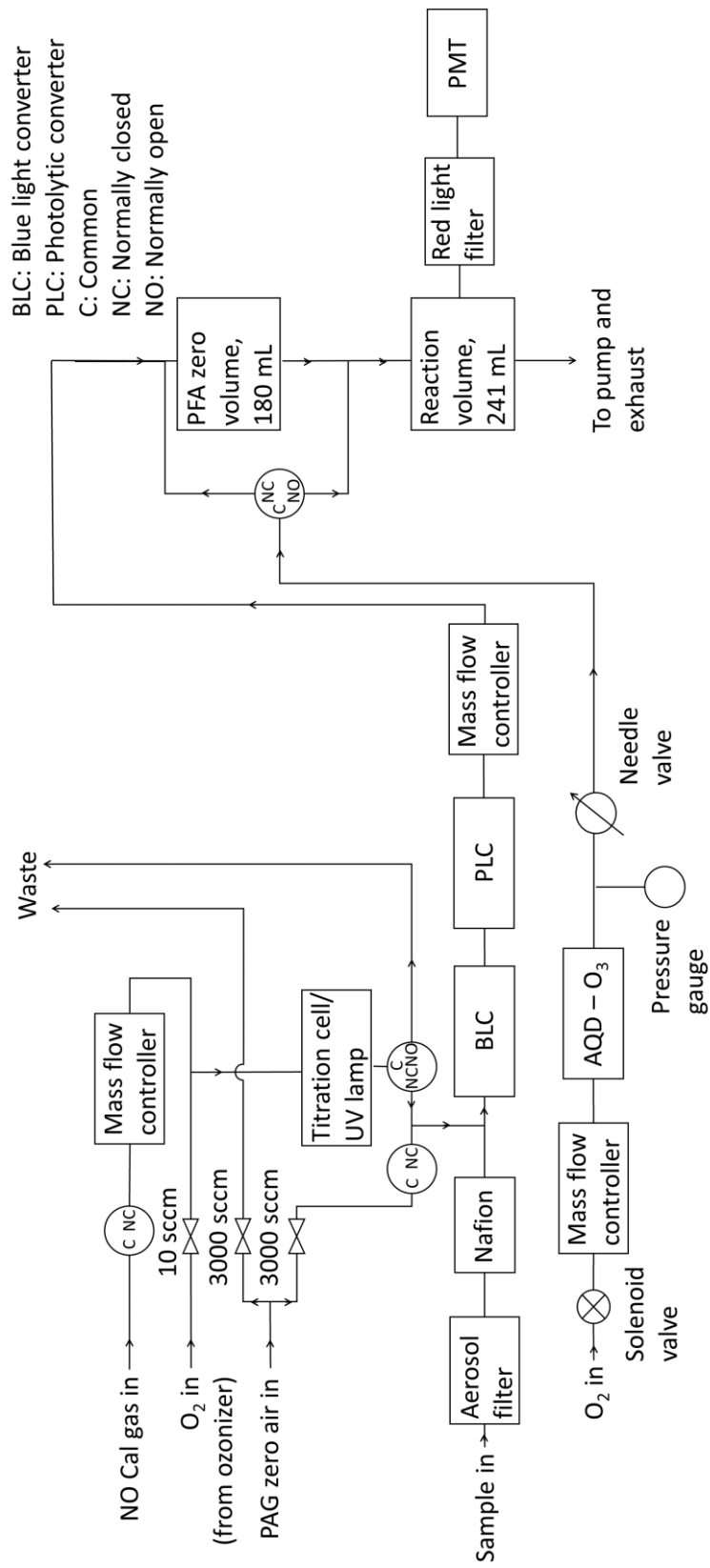


Figure 2: Flow diagram of the NO_x instrument at the CVAO.

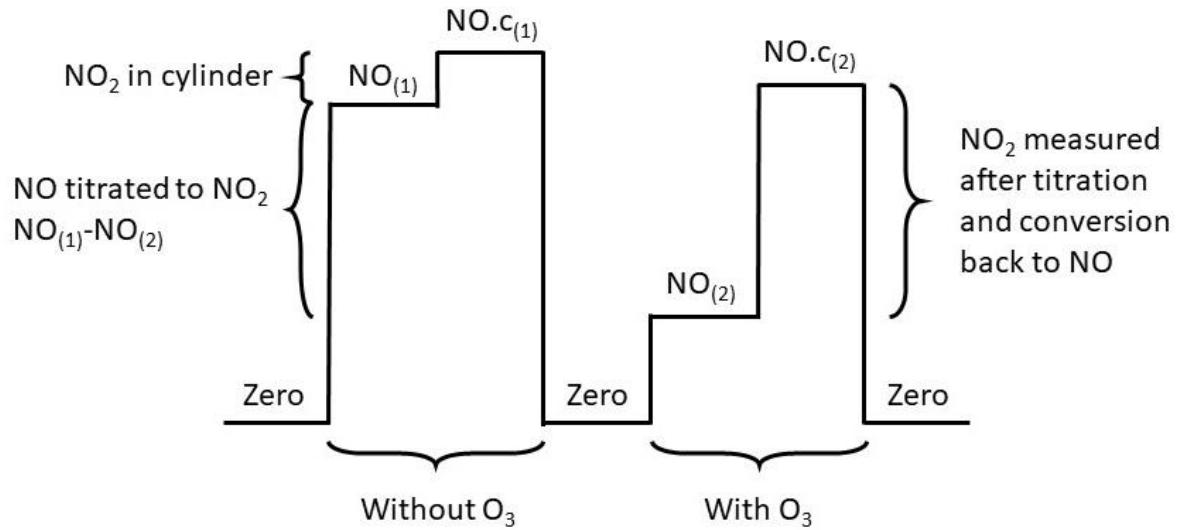


Figure 3: A theoretical calibration cycle. "NO" is the measurement of only NO i.e. when the converters are off, NO.c is when one of the converters are on therefore the measurement is NO + NO₂ and (1) and (2) represent untitrated and titrated NO, respectively.

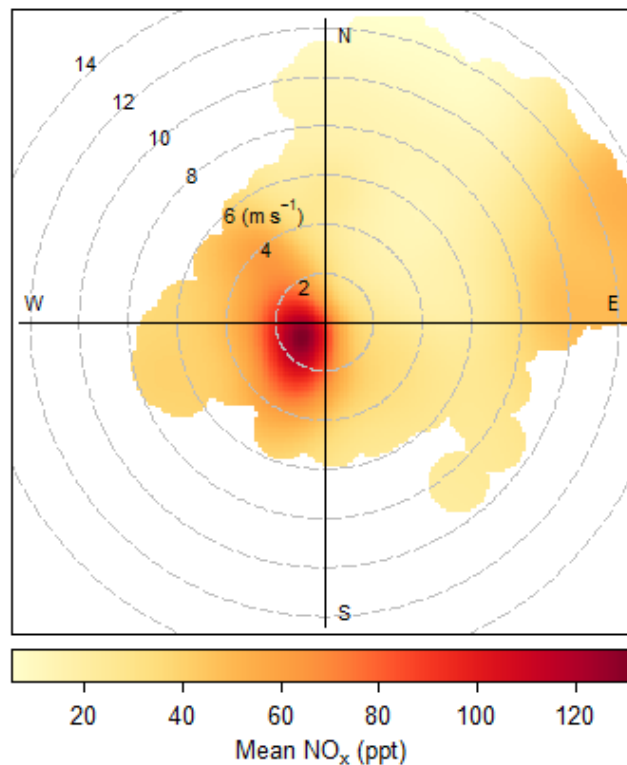


Figure 4: Total NO_x from June 2017 to August 2019 plotted as a function of wind speed and direction.

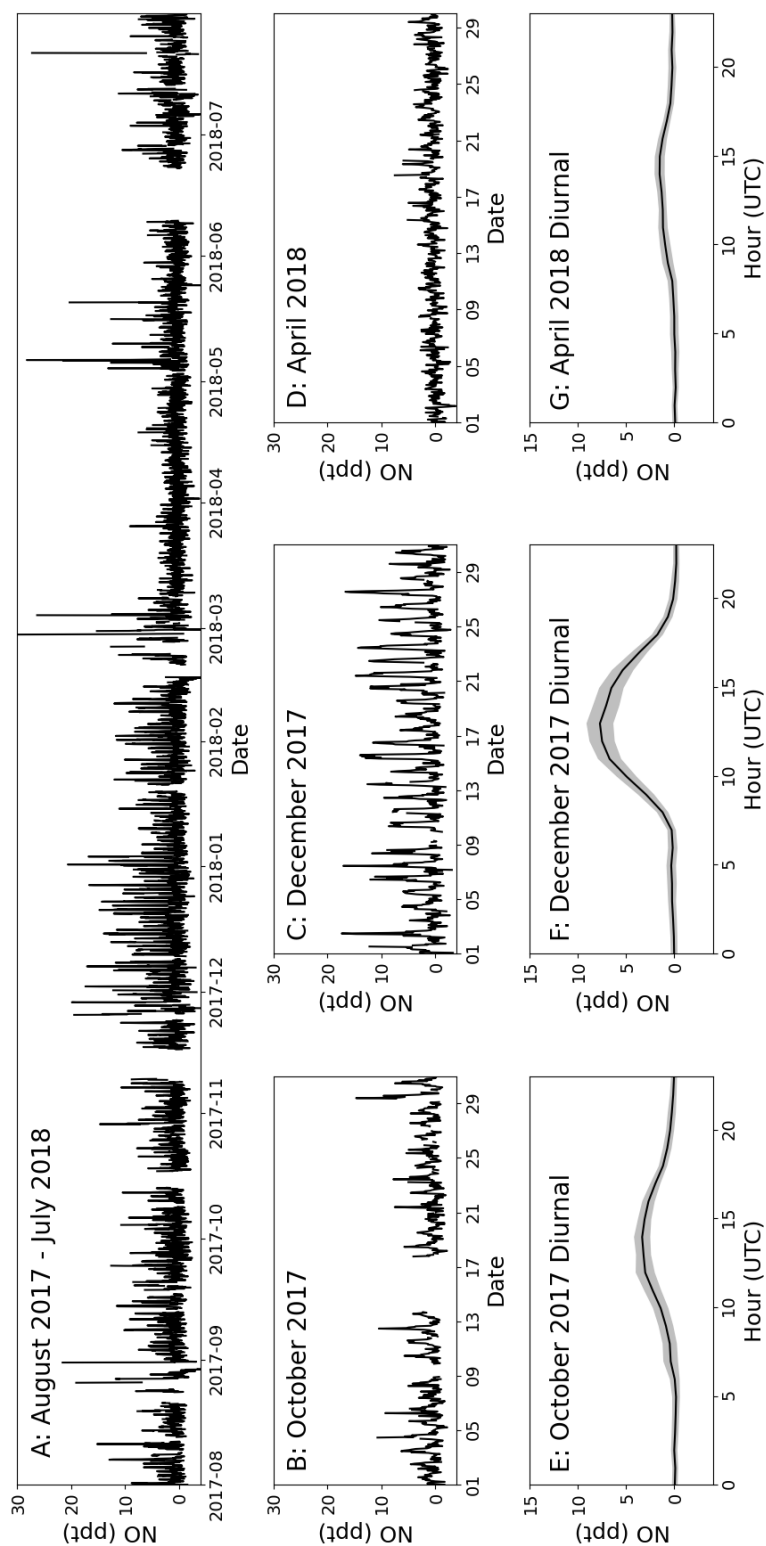


Figure 5: Panel A show the time series for filtered O_3 corrected NO from August 1st 2017 to July 31st 2018. Panel B, C and D zoom in on October 2017, December 2017 and April 2018, respectively. Panel E, F and G show the average diurnal of NO for October 2017, December 2017 and April 2018, respectively, with the coloured areas being ± 2 standard errors. If there are less than 15 measurements available for the hour, it is not included in the diurnal.

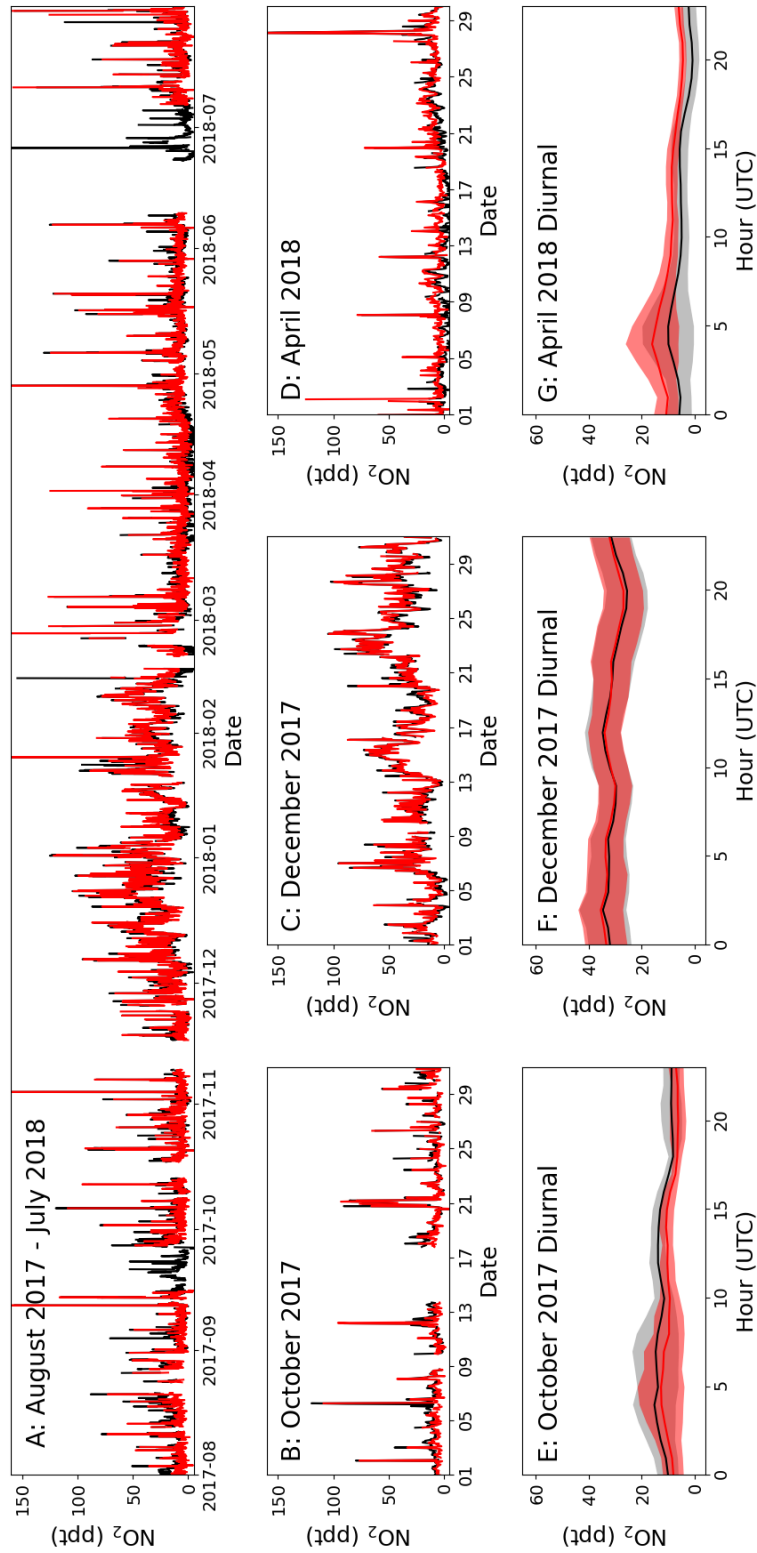


Figure 6: Panel A show the time series of filtered O₃ corrected NO₂ from August 1st 2017 to July 31st 2018 for the BLC (black) and PLC (red). Panel B, C and D zoom in on October 2017, December 2017 and April 2018, respectively, with the red line being the PLC and the black being the BLC. Panel E, F and G show the average diurnal of NO₂ for October 2017, December 2017 and April 2018, respectively, with the red line being the PLC and the black being the BLC and the coloured areas being ± 2 standard errors. If there are less than 15 measurements available for the hour, it is not included in the diurnal.

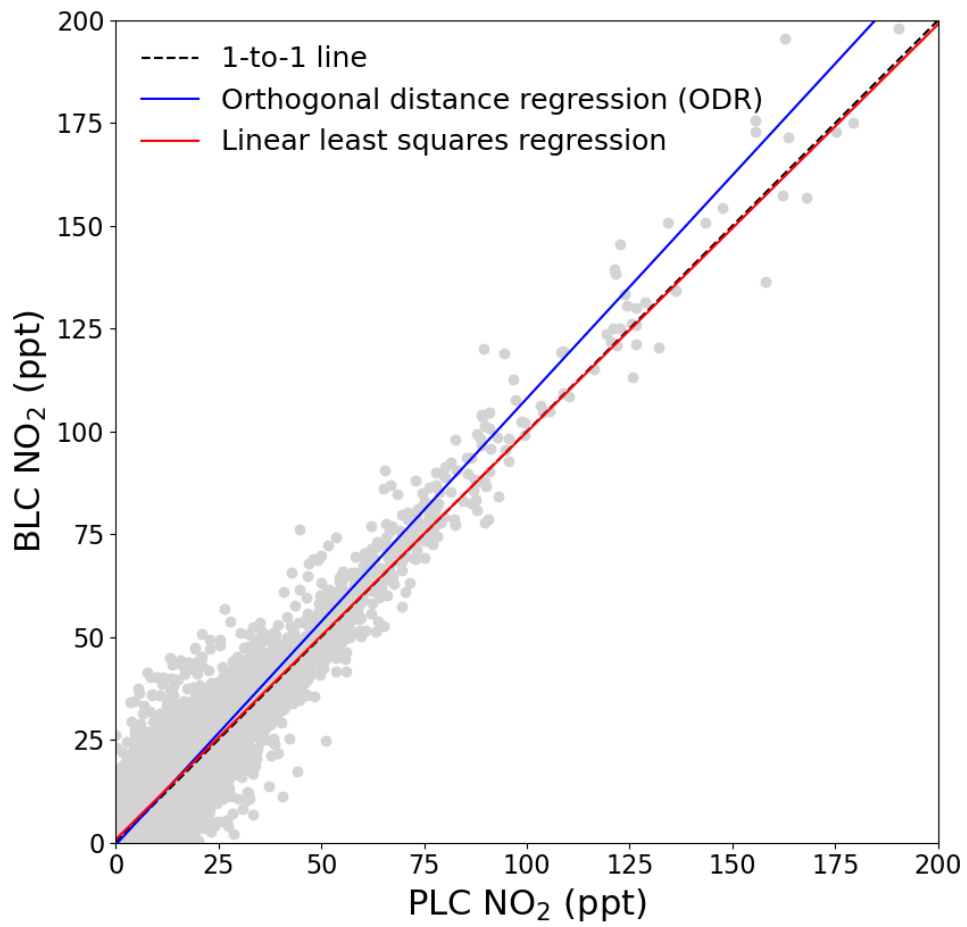


Figure 7: The BLC NO₂ mixing ratio is plotted against the PLC NO₂ mixing ratio. The black dashed line shows the 1-to-1 relationship. The red line is the linear least square regression of the hourly data with uncertainty in y and the blue line is the orthogonal distance regression with uncertainties in both the x and y.

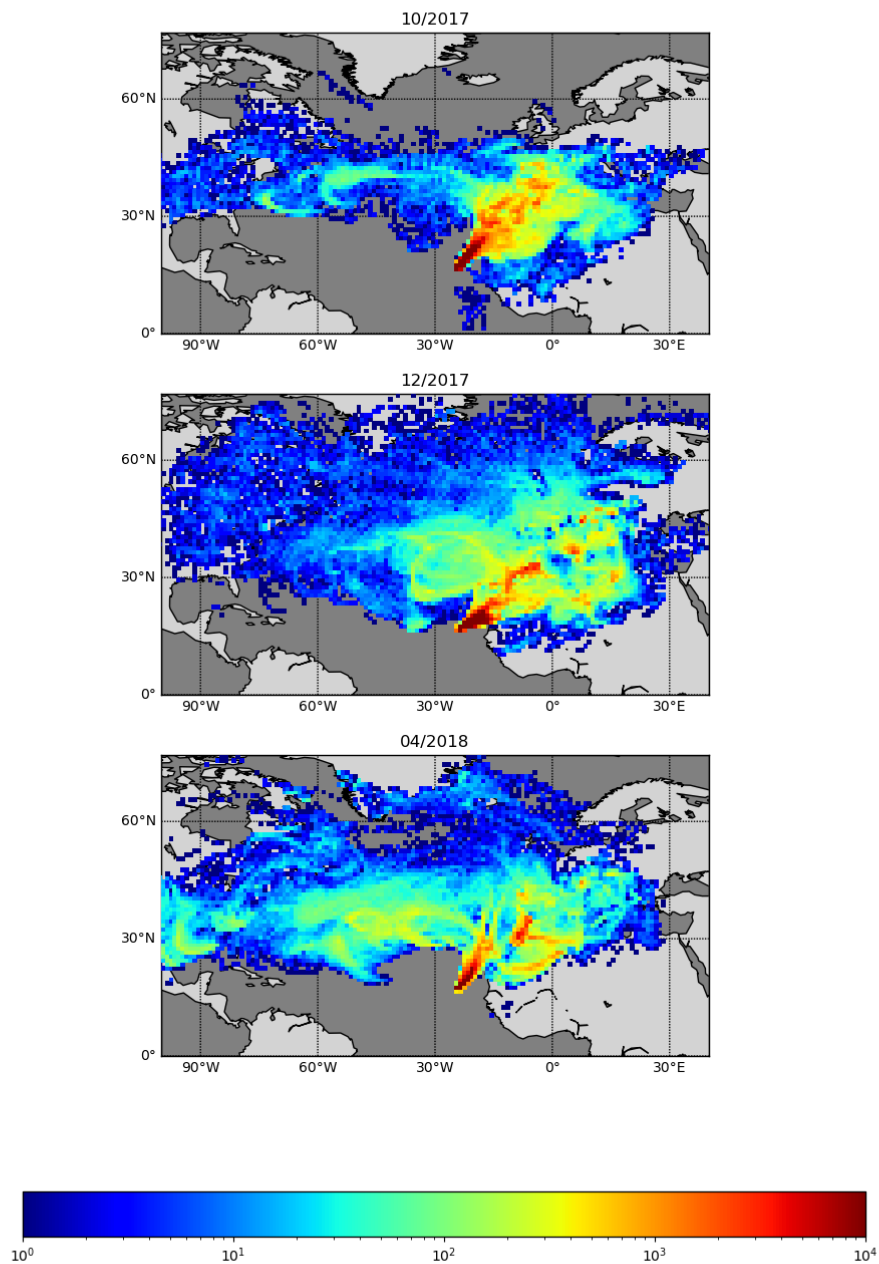


Figure 8: Back trajectories estimated for October 2017, December 2017, and April 2018. FLEXPART version 10.4 is used in backwards mode, driven by pressure level data from Global Forecast System (GFS) reanalyses at $0.5^\circ \times 0.5^\circ$ resolution (Pisso et al., 2019; Stohl et al., 1998). 10-day back-trajectory simulations are initialised every 6 hours, releasing 1000 particles from the CVAO site.

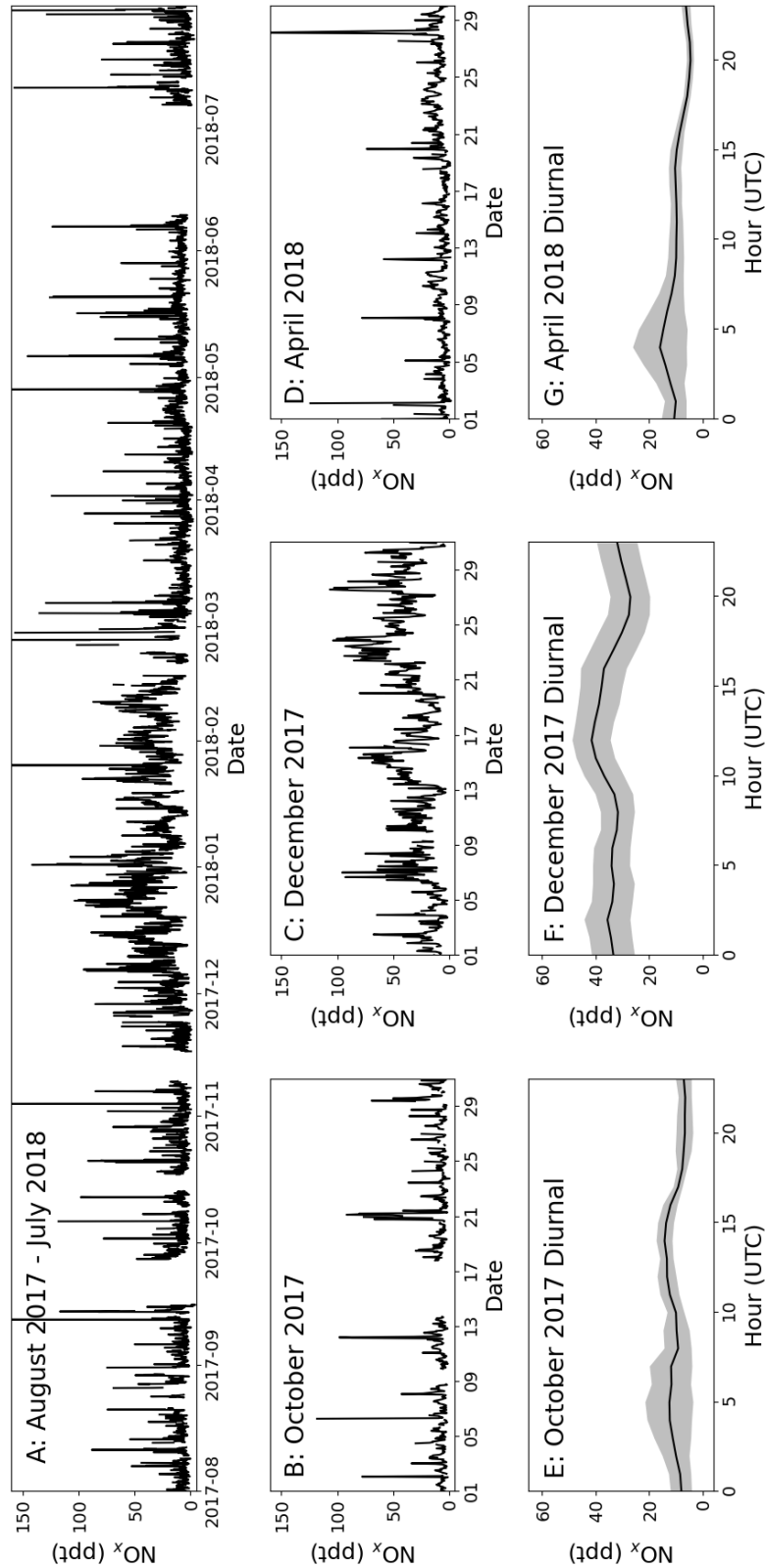


Figure 9: Panel A show the time series for total NO_x (NO + NO₂ PLC) from August 1st 2017 to July 31st 2018. Panel B, C and D zoom in on October 2017, December 2017 and April 2018, respectively. Panel E, F and G show the average diurnal of NO_x for October 2017, December 2017 and April 2018, respectively, with the coloured areas being ±2 standard errors. If there are less than 15 measurements available for the hour, it is not included in the diurnal.

References

- Alam, M. S., Crilley, L. R., Lee, J. D., Kramer, L. J., Pfrang, C., Vázquez-Moreno, M., Muñoz, A., Ródenas, M., and Bloss, W. J.: Interference from alkenes in chemiluminescent NO_x measurements, *Atmos. Meas. Tech. Discuss.*, 2020, 1-26, 10.5194/amt-2020-164, 2020.
- Atkinson, R.: Atmospheric chemistry of VOCs and NO_x, *Atmospheric Environment*, 34, 2063-2101, [https://doi.org/10.1016/S1352-2310\(99\)00460-4](https://doi.org/10.1016/S1352-2310(99)00460-4), 2000.
- Atkinson, R., Baulch, D. L., Cox, R. A., Crowley, J. N., Hampson, R. F., Hynes, R. G., Jenkin, M. E., Rossi, M. J., and Troe, J.: Evaluated kinetic and photochemical data for atmospheric chemistry: Volume I - gas phase reactions of O_x, HO_x, NO_x and SO_x species, *Atmos. Chem. Phys.*, 4, 1461-1738, 10.5194/acp-4-1461-2004, 2004.
- Beine, H. J., Engardt, M., Jaffe, D. A., Hov, Ø., Holme'n, K., and Stordal, F.: Measurements of NO_x and aerosol particles at the NY-A'lesund Zeppelin mountain station on Svalbard: Influence of regional and local pollution sources, *Atmospheric Environment*, 30, 1067-1079, [https://doi.org/10.1016/1352-2310\(95\)00410-6](https://doi.org/10.1016/1352-2310(95)00410-6), 1996.
- Beine, H. J., Honrath, R. E., Dominé, F., Simpson, W. R., and Fuentes, J. D.: NO_x during background and ozone depletion periods at Alert: Fluxes above the snow surface, *Journal of Geophysical Research: Atmospheres*, 107, ACH 7-1-ACH 7-12, 10.1029/2002jd002082, 2002.
- Bell, S.: A Beginner's Guide to Uncertainty of Measurement, National Physical Laboratory (NPL), Teddington, Middlesex, United Kingdom, TW11 0LW, ISSN 1368-6550, 43 pp., 2001.
- Berkes, F., Houben, N., Bundke, U., Franke, H., Pätz, H. W., Rohrer, F., Wahner, A., and Petzold, A.: The IAGOS NO_x instrument – design, operation and first results from deployment aboard passenger aircraft, *Atmos. Meas. Tech.*, 11, 3737-3757, 10.5194/amt-11-3737-2018, 2018.
- Author: Solid-state light source photolytic nitrogen dioxide converter, US 7238328 B2, USA, USPTO, Available at: <https://patents.google.com/patent/US7238328B2> (last access: 18 February 2021), 3 July 2007.
- Carpenter, L. J., Fleming, Z. L., Read, K. A., Lee, J. D., Moller, S. J., Hopkins, J. R., Purvis, R. M., Lewis, A. C., Müller, K., Heinold, B., Herrmann, H., Fomba, K. W., van Pinxteren, D., Müller, C., Tegen, I., Wiedensohler, A., Müller, T., Niedermeier, N., Achterberg, E. P., Patey, M. D., Kozlova, E. A., Heimann, M., Heard, D. E., Plane, J. M. C., Mahajan, A., Oetjen, H., Ingham, T., Stone, D., Whalley, L. K., Evans, M. J., Pilling, M. J., Leigh, R. J., Monks, P. S., Karunaharan, A., Vaughan, S., Arnold, S. R., Tschirner, J., Pöhler, D., Frieß, U., Holla, R., Mendes, L. M., Lopez, H., Faria, B., Manning, A. J., and Wallace, D. W. R. J. J. o. A. C.: Seasonal characteristics of tropical marine boundary layer air measured at the Cape Verde Atmospheric Observatory, 67, 87-140, 10.1007/s10874-011-9206-1, 2010.
- Carroll, M. A., Ridley, B. A., Montzka, D. D., Hubler, G., Walega, J. G., Norton, R. B., Huebert, B. J., and Grahek, F. E.: Measurements of nitric oxide and nitrogen dioxide during the Mauna Loa Observatory Photochemistry Experiment, *Journal of Geophysical Research: Atmospheres*, 97, 10361-10374, 10.1029/91jd02296, 1992.
- Carsey, T. P., Churchill, D. D., Farmer, M. L., Fischer, C. J., Pszeny, A. A., Ross, V. B., Saltzman, E. S., Springer-Young, M., and Bonsang, B.: Nitrogen oxides and ozone production in the North Atlantic marine boundary layer, *Journal of Geophysical Research: Atmospheres*, 102, 10653-10665, 10.1029/96JD03511, 1997.
- Carlsaw, D. C.: Evidence of an increasing NO₂/NO_x emissions ratio from road traffic emissions, *Atmospheric Environment*, 39, 4793-4802, <https://doi.org/10.1016/j.atmosenv.2005.06.023>, 2005.
- Chiapello, I., Bergametti, G., Gomes, L., Chatenet, B., Dulac, F., Pimenta, J., and Soares, E. S.: An additional low layer transport of Sahelian and Saharan dust over the north-eastern Tropical Atlantic, *Geophysical Research Letters*, 22, 3191-3194, 10.1029/95gl03313, 1995.
- Clough, P., and Thrush, B. A.: Mechanism of chemiluminescent reaction between nitric oxide and ozone, *Transactions of the Faraday Society*, 63, 915-925, 1967.

- Clyne, M. A. A., Thrush, B. A., and Wayne, R. P.: Kinetics of the chemiluminescent reaction between nitric oxide and ozone, *Transactions of the Faraday Society*, 60, 359-370, 10.1039/TF9646000359, 1964.
- Drummond, J. W., Volz, A., and Ehhalt, D. H.: An optimized chemiluminescence detector for tropospheric NO measurements, *Journal of Atmospheric Chemistry*, 2, 287-306, 1985.
- Dunlea, E. J., Herndon, S. C., Nelson, D. D., Volkamer, R. M., San Martini, F., Sheehy, P. M., Zahniser, M. S., Shorter, J. H., Wormhoudt, J. C., Lamb, B. K., Allwine, E. J., Gaffney, J. S., Marley, N. A., Grutter, M., Marquez, C., Blanco, S., Cardenas, B., Retama, A., Ramos Villegas, C. R., Kolb, C. E., Molina, L. T., and Molina, M. J.: Evaluation of nitrogen dioxide chemiluminescence monitors in a polluted urban environment, *Atmos. Chem. Phys.*, 7, 2691-2704, 10.5194/acp-7-2691-2007, 2007.
- Finlayson, B. J., Pitts, J. N., and Atkinson, R.: Low-pressure gas-phase ozone-olefin reactions. Chemiluminescence, kinetics, and mechanisms, *Journal of the American Chemical Society*, 96, 5356-5367, 10.1021/ja00824a009, 1974.
- Fomba, K. W., Müller, K., van Pinxteren, D., Poulain, L., van Pinxteren, M., and Herrmann, H.: Long-term chemical characterization of tropical and marine aerosols at the Cape Verde Atmospheric Observatory (CVAO) from 2007 to 2011, *Atmos. Chem. Phys.*, 14, 8883-8904, 10.5194/acp-14-8883-2014, 2014.
- Fontijn, A., Sabadell, A. J., and Ronco, R. J.: Homogeneous chemiluminescent measurement of nitric oxide with ozone. Implications for continuous selective monitoring of gaseous air pollutants, *Analytical chemistry*, 42, 575-579, 1970.
- Galbally, I. E.: Nitrogen Oxides (NO, NO₂, NO_y) measurements at Cape Grim: A technical manual CSIRO, Australia, 119 pp., 2020, <https://doi.org/10.25919/dt6y-3q53>.
- Gilge, S., Plass-Dülmer, C., Rohrer, F., Steinbacher, M., Fjaeraa, A. M., Lagler, F., and Walden, J.: WP4-NA4: Trace gases networking: Volatile organic carbon and nitrogen oxides Deliverable D4.10: Standardized operating procedures (SOPs) for NO_x measurements, ACTRIS, 22 pp., 2014.
- Grosjean, D., and Harrison, J.: Response of chemiluminescence NO_x analyzers and ultraviolet ozone analyzers to organic air pollutants, *Environmental Science & Technology*, 19, 862-865, 10.1021/es00139a016, 1985.
- Jaeglé, L., Jacob, D. J., Brune, W. H., Tan, D., Faloona, I. C., Weinheimer, A. J., Ridley, B. A., Campos, T. L., and Sachse, G. W.: Sources of HO_x and production of ozone in the upper troposphere over the United States, *Geophysical Research Letters*, 25, 1709-1712, 10.1029/98gl00041, 1998.
- Jones, A. E., Weller, R., Minikin, A., Wolff, E. W., Sturges, W. T., McIntyre, H. P., Leonard, S. R., Schrems, O., and Bauguitte, S.: Oxidized nitrogen chemistry and speciation in the Antarctic troposphere, *Journal of Geophysical Research: Atmospheres*, 104, 21355-21366, 10.1029/1999jd900362, 1999.
- Kley, D., and McFarland, M.: Chemiluminescence detector for NO and NO₂, *Atmos. Technol.:(United States)*, 12, 1980.
- Lee, J. D., Moller, S. J., Read, K. A., Lewis, A. C., Mendes, L., and Carpenter, L. J.: Year-round measurements of nitrogen oxides and ozone in the tropical North Atlantic marine boundary layer, *J Journal of Geophysical Research: Atmospheres*, 114, 2009.
- Logan, J. A.: Tropospheric ozone: Seasonal behavior, trends, and anthropogenic influence, 90, 10463-10482, doi:10.1029/JD090iD06p10463, 1985.
- Matthews, R. D., Sawyer, R. F., and Schefer, R. W.: Interferences in chemiluminescent measurement of nitric oxide and nitrogen dioxide emissions from combustion systems, *Environmental Science & Technology*, 11, 1092-1096, 10.1021/es60135a005, 1977.
- Mazzeo, N. A., Venegas, L. E., and Choren, H.: Analysis of NO, NO₂, O₃ and NO_x concentrations measured at a green area of Buenos Aires City during wintertime, *Atmospheric Environment*, 39, 3055-3068, <https://doi.org/10.1016/j.atmosenv.2005.01.029>, 2005.
- Monks, P. S., Carpenter, L. J., Penkett, S. A., Ayers, G. P., Gillett, R. W., Galbally, I. E., and Meyer, C. P.: Fundamental ozone photochemistry in the remote marine boundary layer: the soapex experiment, measurement and theory, *Atmospheric Environment*, 32, 3647-3664, [https://doi.org/10.1016/S1352-2310\(98\)00084-3](https://doi.org/10.1016/S1352-2310(98)00084-3), 1998.

- Pandey, S. K., Kim, K.-H., Chung, S.-Y., Cho, S. J., Kim, M. Y., and Shon, Z.-H.: Long-term study of NO_x behavior at urban roadside and background locations in Seoul, Korea, *Atmospheric Environment*, 42, 607-622, <https://doi.org/10.1016/j.atmosenv.2007.10.015>, 2008.
- Peterson, M. C., and Honrath, R. E.: NO_x and NO_y over the northwestern North Atlantic: Measurements and measurement accuracy, *Journal of Geophysical Research: Atmospheres*, 104, 11695-11707, 1999.
- Pisso, I., Sollum, E., Grythe, H., Kristiansen, N. I., Cassiani, M., Eckhardt, S., Arnold, D., Morton, D., Thompson, R. L., Groot Zwaftink, C. D., Evangeliou, N., Sodemann, H., Haimberger, L., Henne, S., Brunner, D., Burkhardt, J. F., Fouilloux, A., Brioude, J., Philipp, A., Seibert, P., and Stohl, A.: The Lagrangian particle dispersion model FLEXPART version 10.4, *Geosci. Model Dev.*, 12, 4955-4997, [10.5194/gmd-12-4955-2019](https://doi.org/10.5194/gmd-12-4955-2019), 2019.
- Pollack, I. B., Lerner, B. M., and Ryerson, T. B.: Evaluation of ultraviolet light-emitting diodes for detection of atmospheric NO₂ by photolysis - chemiluminescence, *Journal of Atmospheric Chemistry*, 65, 111-125, [10.1007/s10874-011-9184-3](https://doi.org/10.1007/s10874-011-9184-3), 2010.
- Read, K. A., Mahajan, A. S., Carpenter, L. J., Evans, M. J., Faria, B. V. E., Heard, D. E., Hopkins, J. R., Lee, J. D., Moller, S. J., Lewis, A. C., Mendes, L., McQuaid, J. B., Oetjen, H., Saiz-Lopez, A., Pilling, M. J., and Plane, J. M. C.: Extensive halogen-mediated ozone destruction over the tropical Atlantic Ocean, *Nature*, 453, 1232, [10.1038/nature07035](https://doi.org/10.1038/nature07035)
<https://www.nature.com/articles/nature07035#supplementary-information>, 2008.
- Reed, C., Evans, M. J., Carlo, P. D., Lee, J. D., Carpenter, L. J. J. A. C., and Physics: Interferences in photolytic NO₂ measurements: explanation for an apparent missing oxidant?, 16, 4707-4724, 2016.
- Reed, C., Evans, M. J., Crilley, L. R., Bloss, W. J., Sherwen, T., Read, K. A., Lee, J. D., and Carpenter, L. J.: Evidence for renoxification in the tropical marine boundary layer, *Atmos. Chem. Phys.*, 17, 4081-4092, [10.5194/acp-17-4081-2017](https://doi.org/10.5194/acp-17-4081-2017), 2017.
- Rhoads, K. P., Kelley, P., Dickerson, R. R., Carsey, T. P., Farmer, M., Savoie, D. L., and Prospero, J. M.: Composition of the troposphere over the Indian Ocean during the monsoonal transition, *Journal of Geophysical Research: Atmospheres*, 102, 18981-18995, [10.1029/97JD01078](https://doi.org/10.1029/97JD01078), 1997.
- Ridley, B. A., Carroll, M. A., and Gregory, G. L.: Measurements of nitric oxide in the boundary layer and free troposphere over the Pacific Ocean, *Journal of Geophysical Research: Atmospheres*, 92, 2025-2047, [10.1029/JD092iD02p02025](https://doi.org/10.1029/JD092iD02p02025), 1987.
- Ridley, B. A., and Grahek, F. E.: A Small, Low Flow, High Sensitivity Reaction Vessel for NO Chemiluminescence Detectors, *Journal of Atmospheric and Oceanic Technology*, 7, 307-311, [10.1175/1520-0426\(1990\)007<0307:Aslfhs>2.0.Co;2](https://doi.org/10.1175/1520-0426(1990)007<0307:Aslfhs>2.0.Co;2), 1990.
- Ridley, B. A., Grahek, F. E., and Walega, J. G.: A Small High-Sensitivity, Medium-Response Ozone Detector Suitable for Measurements from Light Aircraft, *Journal of Atmospheric and Oceanic Technology*, 9, 142-148, [10.1175/1520-0426\(1992\)009<0142:Ashsmr>2.0.Co;2](https://doi.org/10.1175/1520-0426(1992)009<0142:Ashsmr>2.0.Co;2), 1992.
- Rijkenberg, M. J. A., Powell, C. F., Dall'Osto, M., Nielsdottir, M. C., Patey, M. D., Hill, P. G., Baker, A. R., Jickells, T. D., Harrison, R. M., and Achterberg, E. P.: Changes in iron speciation following a Saharan dust event in the tropical North Atlantic Ocean, *Marine Chemistry*, 110, 56-67, <https://doi.org/10.1016/j.marchem.2008.02.006>, 2008.
- Ryall, D. B., Derwent, R. G., Manning, A. J., Simmonds, P., and O'Doherty, S.: Estimating source regions of European emissions of trace gases from observations at Mace Head, 2507-2523 pp., 2001.
- Ryerson, T. B., Williams, E. J., and Fehsenfeld, F. C.: An efficient photolysis system for fast-response NO₂ measurements, *Journal of Geophysical Research: Atmospheres*, 105, 26447-26461, [10.1029/2000jd900389](https://doi.org/10.1029/2000jd900389), 2000.
- Stohl, A., Hittenberger, M., and Wotawa, G.: Validation of the lagrangian particle dispersion model FLEXPART against large-scale tracer experiment data, *Atmospheric Environment*, 32, 4245-4264, [https://doi.org/10.1016/S1352-2310\(98\)00184-8](https://doi.org/10.1016/S1352-2310(98)00184-8), 1998.

- Torres, A. L., and Thompson, A. M.: Nitric oxide in the equatorial Pacific boundary layer: SAGA 3 measurements, *Journal of Geophysical Research: Atmospheres*, 98, 16949-16954, 10.1029/92jd01906, 1993.
- Val Martin, M., Honrath, R., Owen, R. C., Pfister, G., Fialho, P., and Barata, F. J. J. o. G. R. A.: Significant enhancements of nitrogen oxides, black carbon, and ozone in the North Atlantic lower free troposphere resulting from North American boreal wildfires, 111, 2006.
- Val Martin, M., Honrath, R. E., Owen, R. C., and Li, Q. B.: Seasonal variation of nitrogen oxides in the central North Atlantic lower free troposphere, *Journal of Geophysical Research: Atmospheres*, 113, 10.1029/2007jd009688, 2008.
- Winer, A. M., Peters, J. W., Smith, J. P., and Pitts, J. N.: Response of commercial chemiluminescent nitric oxide-nitrogen dioxide analyzers to other nitrogen-containing compounds, *Environmental Science & Technology*, 8, 1118-1121, 10.1021/es60098a004, 1974.